Functional Characterization of Ice Plant SKD1, an AAA-Type ATPase Associated with the Endoplasmic Reticulum-Golgi Network, and Its Role in Adaptation to Salt Stress[1][W]

Yingtzy Jou[2], Chih-Pin Chiang[2], Guang-Yuh Jauh, and Hungchen Emilie Yen*

Department of Life Sciences, National Chung Hsing University, Taichung, Taiwan 40227 (Y.J., C.P.C., H.E.Y.); and Institute of Plant and Microbial Biology, Academia Sinica, Nankang, Taipei, Taiwan 11529 (G.Y.J.)

A salt-induced gene *mcSKD1* (suppressor of K^+ transport growth defect) able to facilitate K^+ uptake has previously been identified from the halophyte ice plant (*Mesembryanthemum crystallinum*). The sequence of mcSKD1 is homologous to vacuolar protein sorting 4, an ATPase associated with a variety of cellular activities-type ATPase that participates in the sorting of vacuolar proteins into multivesicular bodies in yeast (*Saccharomyces cerevisiae*). Recombinant mcSKD1 exhibited ATP hydrolytic activities in vitro with a half-maximal rate at an ATP concentration of 1.25 mM. Point mutations on active site residues abolished its ATPase activity. ADP is both a product and a strong inhibitor of the reaction. ADP-binding form of mcSDK1 greatly reduced its catalytic activity. The mcSKD1 protein accumulated ubiquitously in both vegetative and reproductive parts of plants. Highest accumulation was observed in cells actively engaging in the secretory processes, such as bladder cells of leaf epidermis. Membrane fractionation and double-labeling immunofluorescence showed the predominant localization of mcSKD1 in the endoplasmic reticulum-Golgi network. Immunoelectron microscopy identified the formation of mcSKD1 proteins into small aggregates in the cytosol and associated with membrane continuum within the endomembrane compartments. These results indicated that this ATPase participates in the endoplasmic reticulum-Golgi mediated protein sorting machinery for both housekeeping function and compartmentalization of excess Na^+ under high salinity.

Ice plant (*Mesembryanthemum crystallinum*) is an inducible halophyte and Crassulacean acid metabolism (CAM) plant. The induction of CAM at a late juvenile stage is an adaptation to drought and salinity (for review, see Cushman, 2001). The day/night fluctuation of malate content is the main characteristic of the CAM cycle. Malate is synthesized by nocturnal CO_2 fixation and is transported into the vacuole via malate transporters (Hafke et al., 2003). In addition to CAM induction, ice plants are able to sequester excess Na^+ into the vacuole. Epidermal bladder cells (BCs) are the major sites to compartmentalize salt within their huge central vacuoles. This process is initiated by high salinity conditions and enabled by a salt-induced Na^+/H^+ antiporter located in the tonoplast (Barkla et al., 2002). The energy required for this active transport is mainly provided by vacuolar (V)-type ATPase and the expression of certain salt-induced V-ATPase subunits has been reported (Golldack and Dietz, 2001; Kluge et al., 2003). Under salt stress, an increase in the diameter of tonoplast-derived vesicles resulted largely from an increase in V-type ATPase (Rockel et al., 1994). Recently, Epimashko et al. (2004) discovered two types of functionally distinct vacuoles in salt-treated ice plant mesophyll cells: salt storing and malate cycling. The development of functionally distinct vacuoles is achieved presumably by precise and efficient protein sorting machinery, i.e. targeting Na^+/H^+ antiporter to the Na^+ storage vacuole and malate transporter to the malate storage vacuole. The mechanism of vacuolar protein trafficking in ice plants remains largely unknown.

SNAREs, a complex vesicle-mediated transport system, are responsible for the delivery of proteins and lipids to different subcellular organelles. Fusion between vesicles and target membranes is driven by protein-protein interactions between vesicle (v)-SNARE and target (t)-SNARE (for review, see Pratelli et al., 2004). A study by Leyman et al. (2000) showed that the expression of a plasma membrane-localized t-SNARE protein Nt-Syr1 can be induced by 300 mM NaCl in tobacco (*Nicotiana tabacum*) leaves. Mutational defect to the OSM/SPY61 gene, a t-SNARE that mediates vesicle transport from the trans-Golgi to prevacuolar compartments (PVC) in Arabidopsis (*Arabidopsis thaliana*) produces a salt-sensitive phenotype (Zhu et al., 2002). Much less is known about the expression of v-SNARE and SNARE-associated elements under salt stress.

SKD (suppressor of K$^+$ transport growth defect) were first identified by screening mouse cDNA library for the heterologous suppression of the K$^+$-uptake-defect yeast (*Saccharomyces cerevisiae*) phenotype (Périer et al., 1994). Two homologous cDNAs were isolated during the screen and named *SKD1* and *SKD2*. The mammalian *SKD1* was involved in intracellular cholesterol and protein trafficking (Scheuring et al., 1999; Bishop and Woodman, 2000; Lin et al., 2005). The *SKD2* was mammalian *NSF* (*N*-ethylmaleimide sensitive factor), a gene encoding an ATPase that drives the dissociation and reactivation of SNARE complexes. Both SKD1 and SKD2 contain a highly conserved ATPase domain and belong to a protein superfamily called ATPase associated with a variety of cellular activities (AAA) proteins. Cluster and phylogenetic analysis of 1,241 sequences of AAA proteins suggest the existence of six major clades of AAA domains, and SKD1 proteins belong to the meiotic clade (Frickey and Lupas, 2004). AAA proteins function as molecular motors involved in diverse cellular functions including vesicle trafficking, proteosome-mediated protein degradation, and chaperone-like activity (for review, see Hanson and Whiteheart, 2005).

A salt-induced cDNA *mcSKD1* was isolated from salt-treated ice plants by suppression subtractive hybridization (Yen et al., 2000) and found capable of complementing the K$^+$-uptake-defect phenotype and increasing the salt tolerance of yeast mutants (Jou et al., 2004). A database search revealed that both Arabidopsis and rice (*Oryza sativa*) contain one copy of the *SKD1* gene in their genome, yet no study has been done in these two model plants. Vacuolar protein sorting 4 (VPS4), the SKD1 homolog in yeast, plays an essential role in the final step of protein sorting from late endosome to multivesicular bodies (Babst et al., 2002). Recently, Hislop et al. (2004) found mammalian SKD1 to be essential for the down-regulation of mammalian epidermal growth factor receptors by internalization of receptors via endocytosis followed by sorting to lysosomes. SKD1 proteins seem to exist ubiquitously among eukaryotes and are involved in several processes of intracellular vesicle trafficking.

In this report, we first characterized the enzymatic properties of mcSKD1 and then analyzed the accumulation of mcSKD1 at cellular and subcellular levels. This report demonstrated ATPase activity and possible regulation in this group of AAA proteins in plants. Evidence for tissue-specific accumulation and subcellular location of SKD1 is also provided in this study.

RESULTS

Catalytic Properties of mcSKD1

To identify the possible ATPase activity of mcSKD1, the open reading frame of mcSKD1 fused with six His at the C terminus, was cloned into a pET vector, was overexpressed in *Escherichia coli*, and a 51-kD protein was purified by affinity chromatography (Fig. 1A). The N-terminal sequence of the first 10 amino acids exactly matched the N-terminal sequence of mcSKD1. The procedures for mcSKD1 purification were described in "Materials and Methods" and the result was shown in Supplemental Figure 1.

The activity of ATPase was measured by incubation of [α-^{32}P]ATP with crude protein extract isolated from isopropyl-β-D-thiogalactopyranoside (IPTG)-induced *E. coli* cells or affinity-purified mcSKD1 and then separation by thin-layer chromatography (TLC; Fig. 1B). A small amount of ATP was autolyzed into ADP, AMP, and free phosphate during 20 min of incubation at 30°C (lane 1). When crude extract was added to the reaction mixture, a large portion of ATP was converted into ADP and AMP (lane 2). When purified mcSKD1 was used, ATP was essentially converted into ADP and did not further convert to AMP (lane 3). Addition of 5 mM *N*-ethylmaleimide (NEM), a known NSF inhibitor, did not significantly inhibit the enzymatic activity of purified mcSKD1 (lane 4).

The failure to observe inhibition by NEM may be due to the presence of trace amounts of impurity with high ATPase activity in the assay. Therefore, two recombinant proteins with single change in active site residue Lys 177 to Ala (Walker A motif) and Glu 231 to Gln (Walker B motif) were used as negative controls. Residue 177 is critical for ATP binding, while residue 231 is essential for ATP hydrolysis. After going through the same purification steps (Fig. 1A, lanes 4 and 5), the ATPase activities were measured in these two mutants along with the wild-type protein. As shown in Figure 1C, the ATPase activity was reduced 70% in K177A mutant, and the mutation on E231 almost abolished mcSKD1's ATPase activity. The result showed that the activity of ATP hydrolysis detected in our assay system was mostly contributed by mcSKD1.

The enzyme kinetics of affinity-purified mcSKD1 was measured in the range of 0 to 4 mM ATP as substrate. ADP spots of each treatment that appeared on the phosphorimage plate were directly quantified, and the rate of ATP hydrolysis was calculated (Fig. 1D). ATPase activity increased as the substrate concentration increased and reached maximum activity at 3.0 mM ATP. At the half-maximal rate, the ATP concentration was about 1.25 mM. Furthermore, when the ATP concentration exceeded 3.0 mM, ATPase activity rapidly dropped. The inhibition of ATPase activity may be due to the presence of a high level of substrate or the gradual accumulation of product in the reaction mixture.

To further characterize the enzymatic properties of mcSKD1, a competition assay was performed using different nucleotides or deoxynucleotides as competitors (Fig. 2A). In addition to 0.02 μM [α-^{32}P]ATP, an equal amount of nonradioactive nucleotides or deoxynucleotides were added to the reaction mixture. The results showed the presence of ADP caused approximately 50% inhibition of ATPase activity. The inhibitory effect by nonradioactive ATP was much less
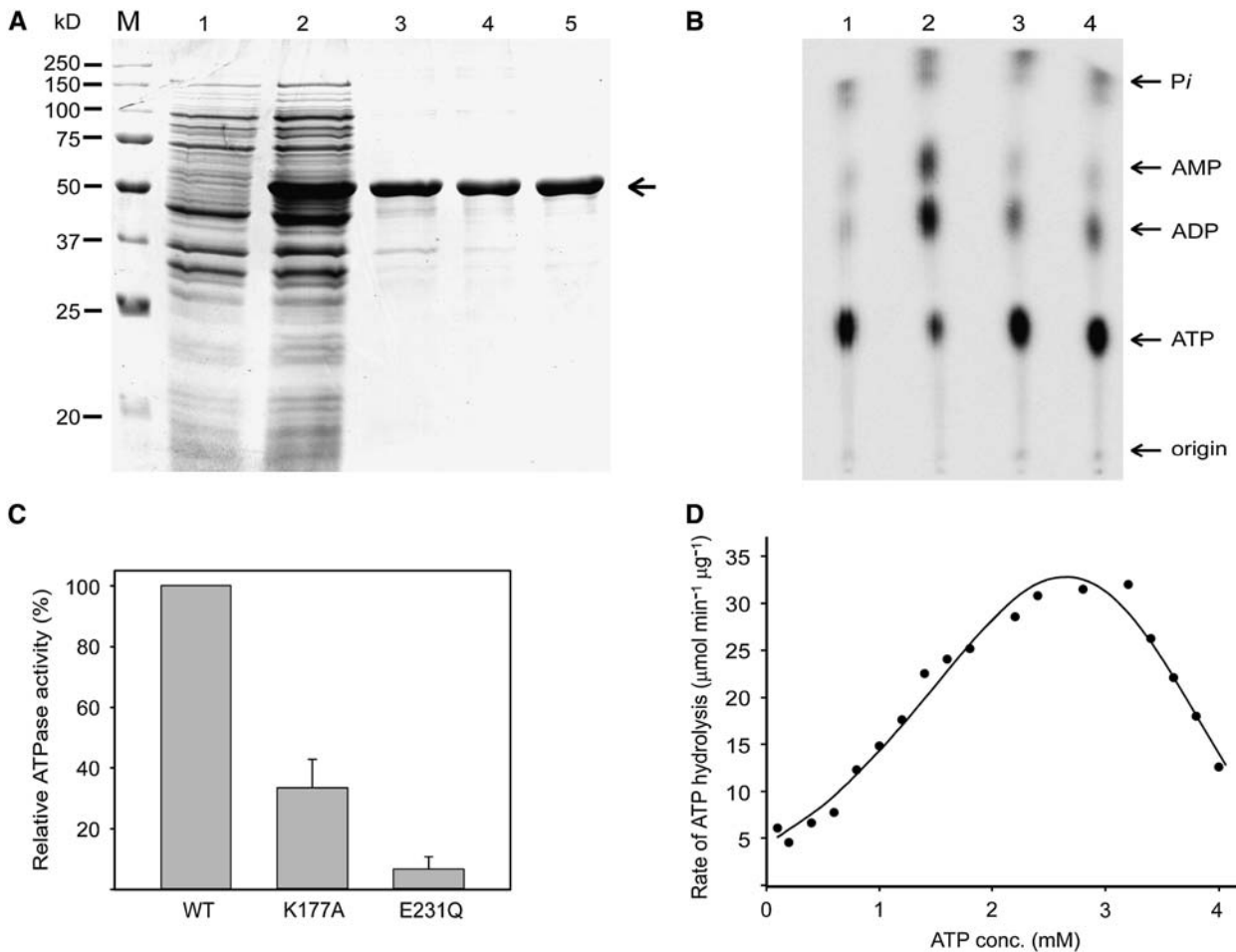
Figure 1. mcSKD1 contains ATPase activity. A, Purification of mcSKD1. The open reading frame of mcSKD1 fused with six His at the C terminus was overexpressed in *E. coli* and purified by Co^{2+} affinity column. Lane1, Total soluble protein before IPTG induction; lane 2, total soluble protein after 2 h IPTG induction; lane 3, purified mcSKD1; lane 4, purified mutant mcSKD1 with Lys 177 changing to Ala; lane 5, purified mutant mcSKD1 with Glu 231 changing to Gln. Proteins were separated by SDS-PAGE and stained with Coomassie Blue. The arrow indicates the position of 51 kD overexpressed protein. M, Protein marker. B, ATPase assay. ATPase activity was measured by incubation proteins with $[\alpha\text{-}^{32}P]ATP$, separated by TLC, and detected by PhosphorImaging. Lane 1, No protein control; lane 2, total soluble protein after 2 h IPTG induction; lane 3, purified mcSKD1; lane 4, purified mcSKD1 plus 5 mM NEM. The ATP concentration was 1.5 mM. Arrows indicate the corresponding positions of adenosine 5′-phosphates and free phosphate (Pi). C, Relative ATPase activity of wild type and mutant mcSKD1. The ATPase activities of purified wild-type mcSKD1 protein and two mutants K177A and E231Q were measured. The condition for ATPase assay was the same as B. The ATPase activity of wild-type mcSKD1 was set as 100%. Data represent means ± SD from three separate experiments. D, Enzyme kinetics. The ATPase activity was measured at 0 to 4 mM ATP and the phosphor image of ADP was quantified using ImagQuant software. The specific activity of ATPase is expressed as μmol ADP produced min^{-1} μg $protein^{-1}$. Data represent means of two independent experiments.

significant. The addition of AMP stimulated about 10% of ATPase activity, while deoxynucleotides had essentially no effect. These results suggested that ADP has a higher affinity for mcSKD1 than substrate ATP and that the ADP-binding form of mcSKD1 loses its catalytic activity.

We further investigated the hypothesis that ADP binding causes inhibition of ATPase activity (Fig. 2B). The enzyme assay was performed at either noninhibitory (1.8 mM ATP) or inhibitory (4.0 mM ATP) conditions. After 20 min incubation, the reaction was stopped and the reaction mixture was divided into two parts. One part was loaded directly on the TLC plate (control), while the other half was filtrated through a Sephadex G50 column before loading onto the TLC plate (centrifugal gel filtration [CGF]). The purpose of CGF was to remove unbounded free nucleotides from the proteins. Results showed that the Sephadex G50 column effectively removed free nucleotides but showed no change to the ATP/ADP ratio in treatments with different ATP concentrations (compare lane 5 versus lane 7) as well as under noninhibitory condition (compare lane 2 versus lane 6). Under inhibitory condition, 20% more ADP was detected
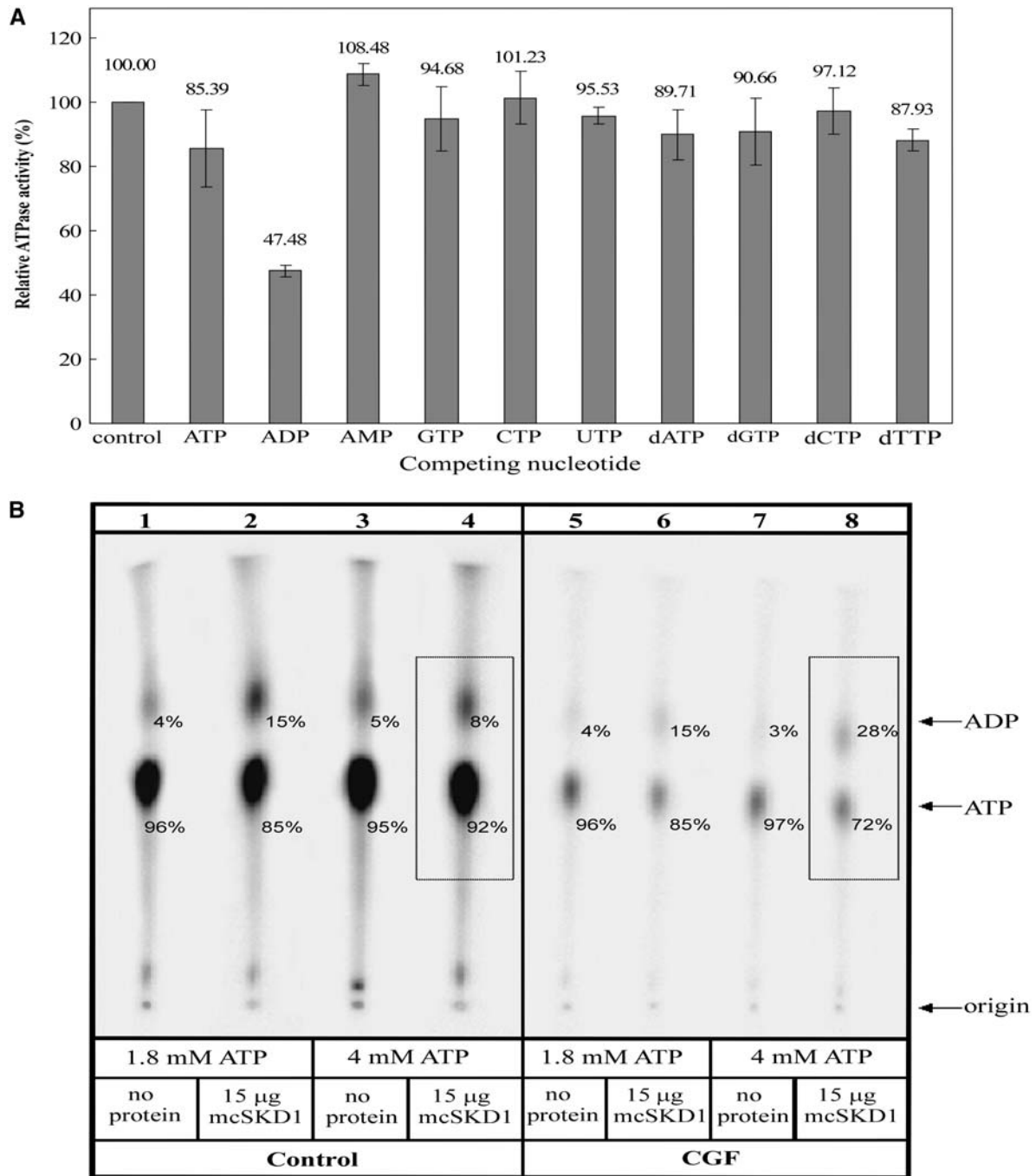
Figure 2. Inhibition of ATPase activity by ADP binding. A, Competition assay. ATPase assay was carried out in the presence of 0.02 μM [α-^{32}P]ATP alone (control) or in the presence of equal molar nonradioactive ADP, AMP, GTP, CTP, UTP, dATP, dGTP, dCTP, or dTTP. The relative ATPase activity was calculated by setting control experiment as 100%. Data represent means $\pm$ SD from three separate experiments. B, Nucleotide binding assay. The mcSKD1 ATPase activity was performed under a noninhibitory ATP concentration (1.8 mM) or an inhibitory ATP concentration (4.0 mM). After reaction, a half volume of solution was run through CGF and another half was taken as the control (Control). Lanes 1, 3, 5, and 7: no protein was added in the reaction mixture; lanes 2, 4, 6, 8: addition of 15 μg affinity-purified mcSKD1. The total phosphorimage of each lane is set as 100%, and the relative intensity of ADP and ATP in each lane is indicated by numbers (%).

following CGF (compare lane 4 versus lane 8). This is because ADP was bound to mcSKD1 and cofractionated through the Sephadex G50 column under inhibitory conditions. The result clearly indicated that this ATPase is subjected to product inhibition. The significance of this finding will be discussed.

Localization of mcSKD1

To assess mcSKD1's function, antiserum raised against purified mcSKD1 was used to identify the localization of this protein in ice plants. Immunoblot analysis showed this antiserum reacted specifically with a 60-kD protein in both vegetative and reproductive organs of ice plants (Fig. 3B). The results showed mcSDK1 ubiquitously accumulated in this halophyte. Salt stress treatment slightly increased its accumulation in the leaves (Fig. 3B). As shown in Figure 1A, the
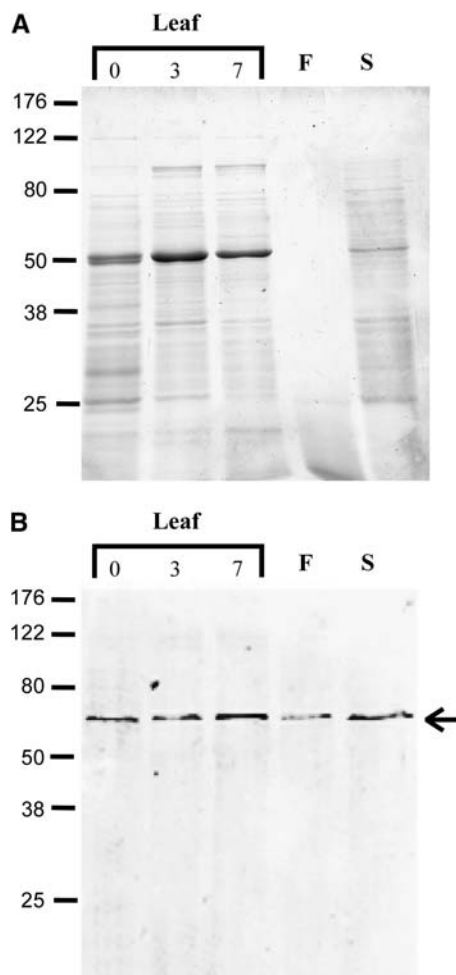

Figure 3. Accumulation of mcSKD1 in plant organs. Total cellular protein extracted from pot-grown 7-week-old leaves (400 mm NaCl treated 0, 3, and 7 d), 10-week-old flowers, and 10-week-old developing seeds were separated by SDS-PAGE (A) and immunoblotting against anti-mcSKD1 antiserum (B). Leaf and seed proteins (50 µg) and flower proteins (5 µg) were loaded per lane. The arrow indicates the position of a 60-kD immunoreactive protein. F, Flower; S, seed.

open reading frame of mcSKD1 encodes a protein with molecular mass of 51 kD. This result suggests that plant SKD1 protein may have some posttranslational modification.

Tissue-specific and salt-induced accumulation of mcSKD1 was examined using immunostaining. Paraffin sections were first reacted with anti-mcSKD1 antibodies and then detected by fluorescein-isothiocyanate (FITC)-conjugated secondary antibodies under fluorescence microscope (Fig. 4). A yellowish fluorescence was detected in all the tissues examined when preimmune antiserum were used as primary antibodies (Fig. 4, A, C, E, and G). This nonspecific autofluorescence was probably caused by phenolic compounds present in the cell wall of mesophyll cells. In salt-treated leaves, mcSKD1 highly accumulated in the epidermal BCs as shown by the emission of green fluorescence (Fig. 4B). Some green fluorescence also emitted from the mesophyll cells but was overlapped with the yellow fluorescence. BCs are major storage sites for excess Na^+ in this halophyte, and large numbers of cisternae of endoplasmic reticulum (ER) were presented in these cells (Kramer, 1979). The accumulation of mcSKD1 was also found in the phloem and cortex of salt-treated roots (Fig. 4D), outer layer of pollen sacs (Fig. 4F), and seed coats (Fig. 4H). All these cells are actively engaged in the secretory processes, either exclusion out of cells, or compartmentalization into the vacuole.

Although the hydropathy plot showed mcSKD1 to have no apparent transmembrane domains (Jou et al., 2004), the mcSKD1 yeast homolog VPS4 associated with the endosomal membrane through protein-protein interactions. Cell fractionation experiment showed mcSKD1 was mainly associated with microsomes but not with soluble fractions (Fig. 5A). Microsomes were further fractionated by Suc gradient. Preliminary fractionation experiment using a 20% to 45% continuous Suc gradient showed mcSKD1 appeared in the very top of the gradient (data not shown). Therefore, a broad range of 8% to 45% gradient was used to separate the relatively light vesicles. Western-blot analysis showed mcSKD1 distributed in the fraction 1 through 7 (8%–34% Suc), mainly in the top four fractions (less than 20% Suc). The pattern of mcSKD1 distribution matched with microsomal epoxide hydrolase (mEH), an ER marker, and AtTLG2a, a trans-Golgi network (TGN) marker (Fig. 5B). A less amount of mcSKD1 was detected in microsomes derived from the tonoplast and PVC distributed in denser fractions (34%–45% Suc) as indicated by the tonoplast marker V-type ATPase and PVC markers vacuolar sorting receptor (VSR) and BP-80. The results showed that mcSKD1 is mainly present in microsomes derived from the ER-Golgi network.

The density of tonoplast fraction shown in these cultured cells (34%) was heavier than the density observed in the mesophyll cells (22%; Barkla et al., 1995). This difference was mainly due to the changes of tonoplast density during vacuole development. According to Herman et al. (1994), the density of
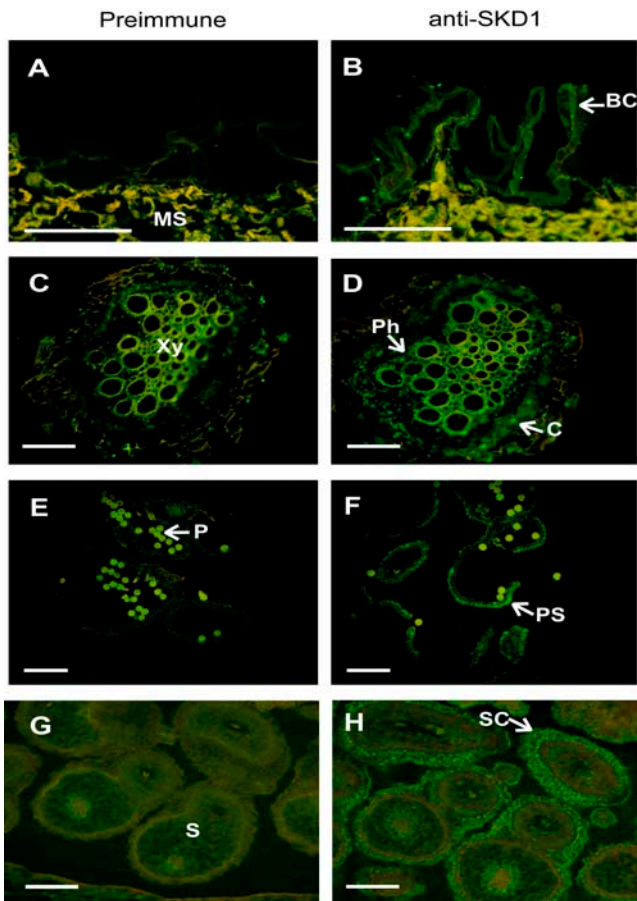
Figure 4. Tissue-specific accumulation of mcSKD1. Paraffin sections were prepared from pot-grown 7-week-old salt-treated leaves (A and B) and roots (C and D), 10-week-old anthers (E and F), and developing seeds (G and H). The accumulation of mcSKD1 protein was detected by immunostaining using preimmune serum (left) or anti-mcSKD1 antiserum (right), followed by FITC-conjugated secondary antibodies. Green fluorescence highlighted the positions where mcSKD1 accumulated (white arrows). The yellowish color indicates autofluorescence emitted by phenolic compounds. BC, Bladder cell; C, cortex; MS, mesophyll cell; Ph, phloem; Xy, xylem; P, pollen; PS, pollen sac; S, seed; SC, seed coat. Bar = 100 μm.

observed when double labeling with tonoplast marker V-type ATPase. The merged image shows punctuate concentrated magenta spots located next to the tonoplast marker. An even lesser degree of colocalization was observed when double labeling with PVC markers BP-80 or VSR. However, we constantly observed some overlapping area as indicated by the white arrowheads (section III). The result obtained by double labeling was consistent with the membrane fractionation study, whereby the majorities of mcSKD1 shared the same location with mEH and AtTLG2a and suggest that mcSKD1 is predominantly gathered in
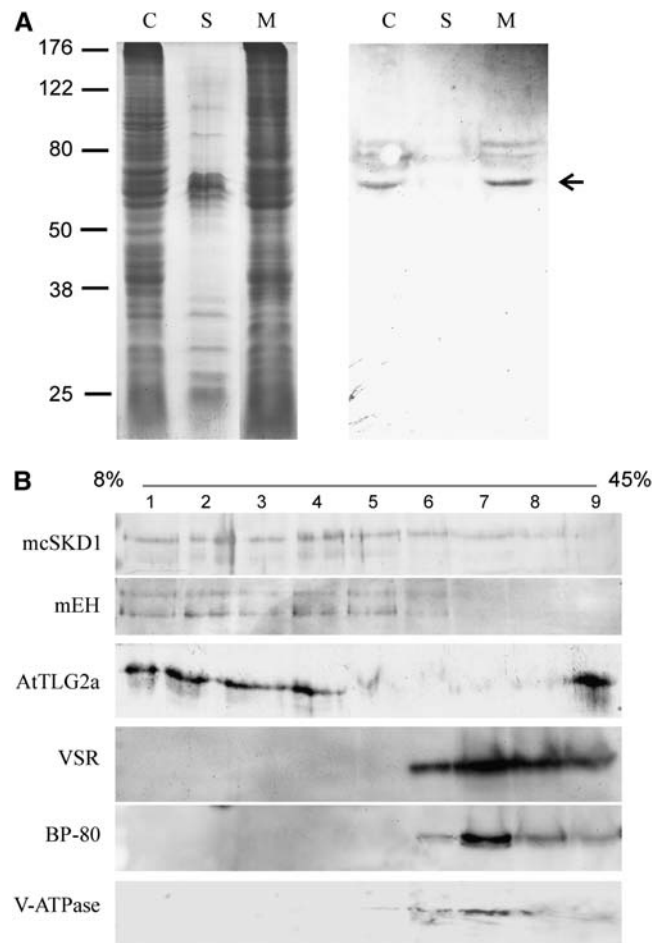

Figure 5. Distribution of mcSKD1 in microsomal fractions. A, Total cellular protein extracted from 10-d-old cultured ice plant cells were separated into soluble (S) and microsomal (M) fractions. Proteins were separated by SDS-PAGE (left) and immunoblotting against anti-mcSKD1 antiserum (right). Fifty micrograms of proteins were loaded per lane. The arrow indicates the position of a 60-kD immunoreactive protein. C, Total cellular protein; S, soluble protein; M, membrane protein. B, Microsomes isolated from cultured ice plant cells were fractionated using a continuous 8% to 45% Suc gradient, and nine fractions (numbers on the top) were collected from top to bottom. The average Suc concentration in each fraction is 11%, 14%, 18%, 20%, 23%, 28%, 34%, 39%, and 42% (w/v), respectively. Membrane proteins in each fraction were separated by SDS-PAGE and immunoblotting against anti-mcSKD1, mEH, anti-AtTLG2a, VSR, anti-BP80, and anti-V-ATPase antibody.

tonoplast in mature root cells was enriched in 20% to 22% Suc, while the density of tonoplast was distributed in the heavier fractions in undifferentiated root tip cells, which lack large central vacuoles.

The localization of mcSKD1 relative to mEH, AtTLG2a, BP-80, VSR, and V-type ATPase in isolated cultured ice plant cells was further examined by double-labeling immunofluorescence (Fig. 6). The magenta fluorescence indicated the distribution of mcSKD1 scattering over the cytoplasm with some concentrated spots (section I). High degrees of colocalization of mcSKD1 with the ER marker mEH and the TGN marker AtTLG2a were observed with 81% and 74%, respectively (section II; green fluorescence). Although the degrees of colocalization were high, there were some distinct spots that appeared only for mcSKD1, as indicated by the magenta arrowheads (section III; merged image). About 40% of colocalization was
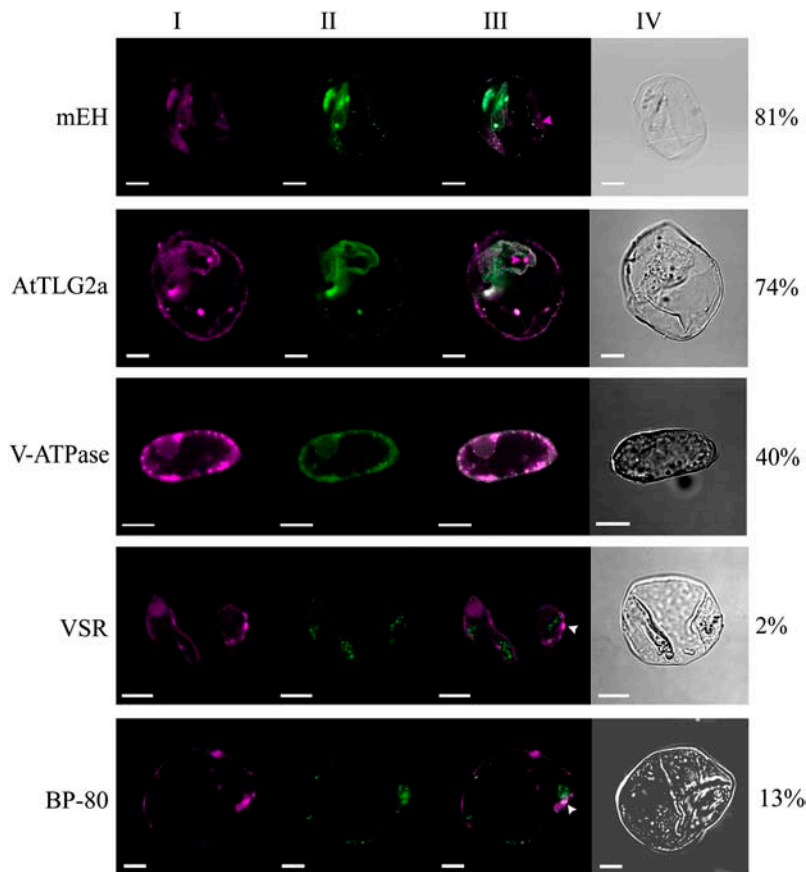
Figure 6. Double-labeling immunofluorescence. Ice plant cells were dual labeled by anti-mcSKD1 and anti-mEH, AtTLG2a, BP-80, VSR, or V-type ATPase. Confocal images represent single images of FITC/rhodamine dual labeling of a representative cell. At least 15 cells were examined in each treatment. The image of mcSKD1 is shown by magenta fluorescence (section I), whereas other markers are indicated by green fluorescence (section II). A merged image of dual labeling is shown in section III, and white color indicates the colocalization area of the two proteins. Section IV is the cell image under Nomarski optics (differential interference contrast). Numbers on the right indicate the percentage of overlapping (white/magenta $\times$ 100%). Magenta arrowheads indicate the nonoverlapping area and white arrowheads indicate the overlapping area.

specific sites of the ER-Golgi network but also occasionally associates with the tonoplast.

To determine the punctuate pattern of mcSKD1, the subcellular localization of mcSKD1 was performed using immunogold labeling (Fig. 7). Ultrathin sections prepared from salt-treated leaves (Fig. 7, A and B), roots (C and D), and cultured cells (E and F) were reacted with preimmune serum or anti-SKD1 antiserum and detected by gold-conjugated anti-rabbit antibodies. In all the tissues examined, mcSKD1 was located in the cytosol in both free form and formation of small aggregates. Under higher magnification, the aggregation of mcSKD1 was found to associate with the cisternal-like membranous structure resembling the ER-Golgi network (Fig. 7B, inset).

DISCUSSION

Efficient Protein Trafficking Is a Salt-Tolerant Determinant

The possible involvement of intracellular vesicle trafficking in maintaining ion homeostasis includes: (1) the delivery of tonoplastic- or plasma membrane-bound transporters, channels, and ATP-driving pumps that directly participate in the ion transport process (Zhu, 2001); (2) the transport of cargo proteins to specific organelles (Slesak et al., 2002) or proteosomes that

facilitate adaptation to high salinity; and (3) the cycling of stress signaling receptors (Katzmann et al., 2002) or membrane compounds (Levine, 2002) that mediate the osmotic stress responses. Therefore, increasing the efficiency of protein trafficking machinery, such as docking, fusion, and recycling, should have positive effects on plant adaptation to a high salinity environment.

There is an increasing amount of evidence for the importance of the machinery of intracellular vesicle trafficking in adaptation to salt stress. For vesicle targeting and docking, small GTPases of the Rab family have been known to be important (for review, see Zerial and McBride, 2001). Overexpression of the Rab GTPase (AtRabG3e) gene in Arabidopsis showed an increase in tolerance to salt and osmotic stresses and reduced accumulation of reactive oxygen species (Mazel et al., 2004). In halophyte ice plants, the expression of a N-myristoylated Rab GTPase was induced by salt stress (Bolte et al., 2000), and this Rab was involved in vesicle transport to the prevacuolar compartment of the lytic vacuole but not to the neutral vacuole (Bolte et al., 2004).

The vesicle fusion process requires the specific pairing of SNAREs (for review, see Pratelli et al., 2004). Leyman et al. (1999) showed that a salt-induced tobacco t-SNARE protein, NtSyr1, was implicated in abscisic acid-mediated stomatal closure, while Geelen et al. (2002) provided evidence for the participation of
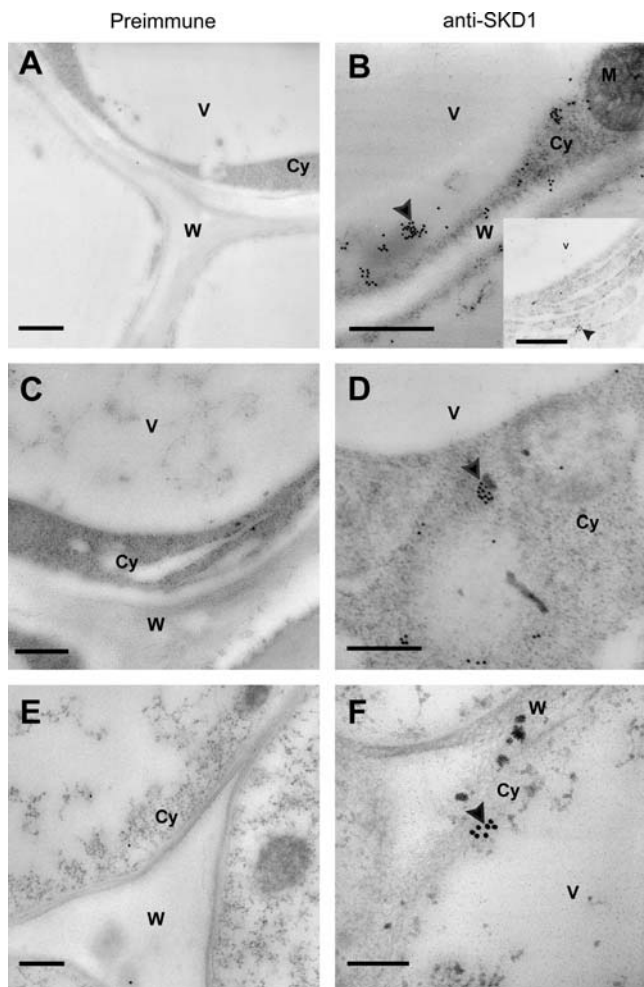
Figure 7. Subcellular localization of mcSKD1. Ultrathin sections obtained from 7-week-old salt-treated leaves (A and B), roots (C and D), and 2-week-old callus (E and F) were labeled with preimmune serum (left) or with anti-mcSKD1 antibody (right) and detected by gold-conjugated anti-rabbit antibodies. Arrows indicate the position of mcSKD1. Bars represent 0.5 μm in A, B, C, and D and 0.2 μm in inset, E, and F. W, Cell wall; V, vacuole; Cy, cytosol; M, mitochondria.

NtSyr1 in SNARE-mediated vesicle trafficking to the plasma membrane. Screening of the Arabidopsis T-DNA insertion library for salt-sensitive mutants identified a salt stress-related t-SNARE protein, OSM1 (Zhu et al., 2002). OSM1 was shown to be involved with transport vesicles from the trans-Golgi to PVC. In this report, we also demonstrated the accumulation of mcSKD1, an NSF-like ATPase functioning in the ER-Golgi network, in cells specialized for water storage and ion compartmentalization. The results suggest that coordination of key players in vesicle fusion and recycling process contributes to the specificity and kinetics of intracellular vesicle trafficking in salt stress tolerance.

Based on the yeast complementation result, the role of *mcSKD1* was proposed as a facilitator of K^+ uptake and promoter of Na^+ sequestering to maintain a high cytoplasmic K^+/Na^+ ratio (Jou et al., 2004). In line with the predicted function of mcSKD1, we found

mcSKD1 protein concentrated on the epidermal BCs (Fig. 4), the major Na^+ storage site in this halophyte. These specialized cells have the highest V-type ATPase activity and Na^+/H^+ exchange rate among tissues in salt-treated ice plants (Barkla et al., 2002). Therefore, in addition to mediating vesicle trafficking in secretory cells of pollen sac and seed coat, mcSKD1 may be involved in a specific transport pathway in the compartmentalization of excess Na^+.

SKD1 Participates in Multiple Routes of Protein Trafficking

A critical point of mcSKD1's function is to understand its role in the trafficking route. Membrane fractionation experiments showed mcSKD1 occurred mainly in the light-density fractions that cofractionated with smooth ER (SER) and TGN markers (Fig. 5). The distribution of mcSKD1 was confirmed by double-labeling immunofluorescence (Fig. 6). Another line of evidence came from Figure 4 where mcSKD1 was highly accumulated in BCs. These specialized cells have been known to contain very high amounts of ER in the cytoplasm (Kramer, 1979). Several mammalian AAA-type ATPases have also been implicated in regulating Golgi assembly (Meyer, 2005) and ER-associated protein degradation (Römisch, 2005). Most of the membrane proteins and secreted proteins are synthesized in the ER, sorted in the Golgi apparatus, and subsequently form transport vesicles that bud from a donor membrane and fuse with a target membrane. The TGN is a major sorting station where trafficking routes diverge to the plasma membrane or the vacuole. The distinct location of mcSKD1 suggests this AAA-type ATPase participates in the TGN sorting event. After formation of transport vesicles, mcSKD1 is recruited to the TGN where this ATPase catalyzes the dissociation and recycling of the sorting complex. The result suggests the importance of increased efficiency at early stage of protein trafficking in salt stress tolerance.

The colocalization with the SER marker shed light on the possible involvement of mcSKD1 in the first sorting event occurring in the ER. Most vesicles that leave the ER are trafficked to the Golgi complex, yet there are additional transport pathways. Some vesicles, such as precursor-accumulating vesicles, bud from the SER bypassing the Golgi on their way to vacuoles (Hara-Nishimura et al., 1998). Based on the ultrastructural observations, Kramer (1979) also suggested that the PVC derived directly from the ER in developing BCs of ice plant. The involvement of mcSKD1 in specific route of ER protein sorting will be the focus in the future.

In yeast, the SKD1 homolog VPS4 mediates protein sorting from endosome to the multivesicular body (MVB; Babst et al., 2002). The role of plant endosomes is still ill defined, as is the role of plant MVB. Recently, Tse et al. (2004) reported the identification of MVB as PVC in plants; therefore, the possible involvement of mcSKD1 in the route of PVC to vacuole was examined

in this study. The results showed the localization of mcSKD1 did not overlap significantly with two PVC markers. Unlike its yeast homolog, the major site of action for mcSKD1 is not in the route of PVC to vacuole. The overall sequence similarity between plant SKD1 and yeast VPS4 is 70% (Yen et al., 2000). The highest degree of conservation (91%) lies in the central region that contains an ATPase domain, while the similarity of N-terminal region is only 54%. The crystal structure of VPS4 central ATPase cassette and C-terminal helix has been reported, yet the poorly ordered N-terminal structures have not been resolved (Scott et al., 2005). The N-terminal coil-coiled domain of VPS4 binds directly to other coil-coiled proteins in the MVB sorting pathway (Babst et al., 2002; Yeo et al., 2003). The sequence analysis suggests the N-terminal coil-coiled domain of plant SKD1 interacts with a set of protein complexes distinct from its yeast homolog. The inconsistency between plant and yeast demonstrates that members of SKD1-like proteins are similar in function but different in specificity.

Evidence provided by this study suggests that mcSKD1 is localized in the cytoplasmic endomembrane system, primarily in the ER-Golgi network. Although the majority of mcSKD1 did not overlap with V-ATPase in the membrane cofractionation experiments (Fig. 5), it showed 40% overlapping localization with V-ATPase by confocal fluorescent microscopy (Fig. 6). V-ATPase is a marker for the tonoplast, but it is also associated with the ER and PVC. The association of V-ATPase with the endomembrane system is most prominent in the undifferentiated cells (Herman et al., 1994). Golldack and Dietz (2001) reported an increased accumulation of V-ATPase subunit E not only at the tonoplast but also in the cytoplasm in salt-treated ice plants. Similar patterns of distribution were found in V-ATPase subunits c and a (Seidel et al., 2004). The localization of V-ATPase subunits in the cytoplasmic endomembrane system indicates they are transported by the intracellular vesicular trafficking system (Ratajczak, 2000) and that a transient association with mcSKD1 may increase the flux of delivering V-ATPase-containing vesicles to the tonoplast in response to salt stress.

Plant SKD1 Is Regulated by Its Nucleotide-Binding State

The molecular mechanism of plant SKD1 in intracellular vesicular trafficking remains unsolved. In yeast, the involvement of VPS4 in sorting endosomal proteins has been studied in depth (Babst et al., 2002). VPS4 assembles into a homo-oligomer, and ATP hydrolysis drives the dissociation of the ubiquitin-mediated protein sorting complexes on the surface of the endosomal membrane. Although we do not know the exact geometric arrangement of mcSKD1 in our in vitro assay system, the recombinant mcSKD1 surely exhibits ATPase activity, and point mutations on critical amino residues K177 and E231 significantly decrease its activity (Fig. 1). Martin et al. (2005) found

that only one active subunit presented in the AAA-type ATPase ClpX hexamer is sufficient to disassemble protein complexes. The demonstration of ATPase activity and association with endomembrane system of mcSKD1 is the first step toward understanding its role in disassembling protein complexes in the endosomal protein trafficking systems.

Babst et al. (1998) reported the kinetic properties of yeast VPS4. Although both mcSKD1 and VPS4 catalyze ATP hydrolysis, there are differences in their catalytic properties. For example, mcSKD1 was insensitive to 5 mM NEM, the concentration that completely inhibited the ATPase activity of VPS4 (Babst et al., 1998). In addition, the curve of substrate dependence was sigmoid for mcSKD1 while the curve was fit into hyperbola for VPS4. The $K_{1/2}$ [ATP] of mcSKD1 was higher than K_m of VPS4 (1.25 versus 0.6 mM), indicating that mcSKD1 has a lower affinity to ATP. The low ATP affinity of mcSKD1 may be the result of differences in the quaternary structure and/or the presence of high concentrations of ADP in the enzyme assay mixture.

ADP is a strong competitor for ATP and it inhibits the activity of ATP hydrolysis by binding to mcSKD1 (Fig. 2). The physiological role of ADP-bound inhibition remains unclear. The release of ADP may be a rate-limiting step, and therefore, a regulatory step for mcSKD1 ATP turnover. Recall the nucleotide exchange between GTP- and GDP-bound states of Rab GTPase (Zhu et al., 2004). The cycle between GTP (active) and GDP (inactive) conformations influences the ability to interact with its effectors, and as a result, regulates the rate of vesicle transport. Since function of Rab GTPase and AAA-type ATPase are both known as molecular motors to assemble and disassemble oligomeric complexes, the ATPase activity of mcSKD1 may also regulate through the ATP- and ADP-bound states. Based on this assumption, the rate of nucleotide exchange and ATP hydrolysis of mcSKD1 should be cooperatively sped up to meet the high rate of protein trafficking under salt stress.

In summary, findings of this study demonstrate the kinetic properties and cellular localization of plant SKD1 protein. Besides the ability to hydrolyze ATP, plant SKD1 has diverged from that of its yeast equivalent in many aspects. The plant SKD1 appears to associate mainly with the ER-Golgi network, and ATPase activity is regulated by ADP binding. SKD1 protein accumulated mostly in cells actively engaging in the secretory pathway in halophyte ice plants. Exposure to high salinity environments requires the efficient and coordinated operation of all stages of intracellular vesicular trafficking in maintaining ion homeostasis and in salt stress signaling.

MATERIALS AND METHODS

Plant Growth Conditions and Callus Culture

Ice plants (*Mesembryanthemum crystallinum*) were grown in mixed soil (humus to vermiculite to sand, 3:1:1, v/v) in a growth chamber with a

16-h-light (800 μmol quanta m^{-2} s^{-1})/8-h-dark period at 30°C/18°C. For salt treatment, 6-week-old plants were treated with 400 mM NaCl for 7 d. Samples from salt-treated plants and 10-week-old nonstressed flowers and developing seeds were collected for immunoblotting and immunolocalization.

Callus of ice plant initiated from hypocotyls of seedlings was maintained in a modified Linsmaier-Bedner and Skoog solid medium as described by Treichel (1986). The growth conditions for callus were the same as previously described (Yen et al., 2000). Two-week-old callus was used for membrane fractionation and immunofluorescence double labeling.

Bacterial Strains and Plasmids

The bacterial strains used in this work were *Escherichia coli* DH5α and BL21 (DE3). Plasmid vector pGEM T-easy (Promega) was used for cloning and pET 32a (Novagen) was used for overexpression of *mcSKD1* gene. pGEM-MCSKD1 was a pGEM T-easy plasmid carrying the *mcSKD1* gene.

Construction of Plasmids

To construct the overexpression system of *mcSKD1*, an *mcSKD1* coding sequence was PCR amplified using plasmid pGEM-MCSKD1 as a template and oligonucleotide primers 5'-CGGCCGCGGGAATTCGATTCATATGTA-CAG-3' (forward) and 5'-GGATCCATCGAAATTATGCAGCCTT-3' (reverse) tailed with *Nde*I and *Bam*HI restriction sites, respectively. The *Nde*I-*Bam*HI fragment was inserted into the corresponding sites of pET32a to give pMCSKD32. The pMCSKD32 was used as a template for generation of point mutations K177A and E231Q using a site-directed mutagenesis kit (Stratagene). The sequences of all constructs were confirmed by DNA sequencing.

Purification of mcSKD1 Protein

An overnight culture of BL21 (DE3) cells harboring pMCSKD32 was diluted 100-fold in 1 L Luria-Bertani medium containing 100 mg L^{-1} ampicillin and incubated at 37°C with shaking. When A_{600} of the culture reached 0.6, IPTG was added to a final concentration of 0.5 mM. After 2 h, the induced cells were harvested by centrifugation and used for purification of the mcSKD1 protein.

All purification steps were carried out at 4°C. IPTG-induced cells were resuspended in 50 mL of equilibration/wash buffer (50 mM sodium phosphate, pH 7.0, 500 mM NaCl, and 5% glycerol) containing 1 mM phenylmethyl sulfonyl fluoride and disrupted by sonication. Cell extract was centrifuged at 13,000g for 30 min. The supernatant was applied to a Co^{2+} affinity column (BD TALON, BD Bio Science). After washing the column with equilibration/wash buffer containing 10 mM imidazole, bound proteins were eluted with equilibration/wash buffer containing continuant 20 to 100 mM imidazole (Supplemental Fig. 1). Fractions containing 40 mM imidazole had the highest amount of mcSKD1 protein. At 70 mM imidazole, the eluent contained mostly mcSKD1. Therefore, fractions containing 70 to 100 mM imidazole were collected and concentrated by an Amicon Ultra PL-30 (Millpore) column. The identity of purified mcSKD1 protein was confirmed by N-terminal sequencing. Protein samples collected from 70 to 100 mM imidazole were directly spotted on a polyvinylidene difluoride membrane and subjected to Edman degradation. The N-terminal sequencing was performed by an ABI 492 automatic protein sequencer (Perkin-Elmer).

Measurement of ATPase Activity

ATPase activity of purified mcSKD1 protein was assayed by TLC described by Babst et al. (1998). Reactions were carried out at 30°C for 20 min in 20 μL of reaction buffer containing 5 mM MgCl$_2$, 0.1 to 4 mM ATP, 25 to 100 nM [α-^{32}P]ATP (3,000 Ci/ mmol), and 1.5 μg purified mcSKD1 protein. Aliquots from reaction mixtures were spotted onto PEI-cellulose F (Merck) and developed in 0.75 M KH$_2$PO$_4$. The spots of isotope-labeled ADP and ATP were visualized by Typhoon 9000 series and quantified by ImageQuant software (Amersham Bioscience). The enzyme activity was expressed as μmol min^{-1} μg protein^{-1}.

For detection of substrate affinity, ATPase activity was assayed with 0.02 μM [α-^{32}P]ATP and equal concentrations of unlabeled nucleotides or deoxynucleotides. The rate of ATP hydrolysis without any competing nucleotide was set as 100%. Effects of competitors were expressed as residual activity of [α-^{32}P]ATP hydrolysis. To investigate the nucleotide occupancy, a nucleotide-binding assay was performed according to Sianidis et al. (2001). Fifteen micrograms of mcSKD1 protein was incubated with 1.8 mM or 4 mM ATP

mixture ([α-^{32}P]ATP: unlabeled ATP = 1:40,000) at 30°C for 20 min. A half volume of the reaction was run through CGF (Sephadex G-50, Amersham Bioscience) and the other half was used as the control. One microliter of the control and 10 μL of the CGF reaction mixtures were assayed by TLC.

Preparation of Anti-mcSKD1 Antibody

SDS-PAGE purified mcSKD1 protein was emulsified with Freund's complete adjuvant and injected intramuscularly into rabbits or mice. After 2 weeks, the animals were boosted with purified mcSKD1 protein emulsified with Freund's incomplete adjuvant. Four boosters were given in this manner at 2-week intervals. The titer of the serum was estimated by western blotting.

Western Blotting

Six-week-old leaves were treated with 400 mM NaCl, and 10-week-old flowers and developing seeds were collected and ground in an extraction buffer (100 mM Tris, pH 7.6, 5 mM MgCl$_2$, 100 mM NaCl, 1 mM phenylmethyl sulfonyl fluoride, and 2 mM leupeptin) using a mortar and pestle. Protein crude extracts were separated on 12% SDS-PAGE and detected mcSKD1 protein by anti-SKD1 antiserum according to standard procedures.

Immunostaining of Paraffin Sections

The ice plant paraffin sections of pot-grown 7-week-old leaves and roots were salt treated for 1 week, and 10-week-old floral organs were prepared as described by Jou et al. (2004). The sections were stained with an anti-mcSKD1 antiserum followed by FITC conjugated anti-rabbit IgG antibody (Jackson ImmunoResearch). Fluorescent images were examined and photographed by a fluorescence microscope (BX 50, Olympus Optical) equipped with a fluorescence excitation filter (excitation/emission at 460/515).

Membrane Fractionation

Two-week-old callus was ground in THM buffer (50 mM Tris, pH 7.5, 10 mM KCl, 1 mM EDTA, and 0.1 mM MgCl$_2$) containing 8% Suc and centrifuged at 30,000g for 1 h to isolate microsomes. Microsomes were fractionated using an 8% to 45% continuous Suc gradient and separated into nine fractions. Membrane proteins in each fraction were separated by SDS-PAGE and immunoblotting against anti-mcSKD1, an ER marker anti-mEH (Galteau et al., 1985), a TGN marker anti-AtTLG2a (Bassham et al., 2000), prevacuolar compartment markers anti-VSR and anti-BP80 (Tse et al., 2004), and a tonoplast marker anti-V-type ATPase B1 subunit (sc-20943, Santa Cruz Biotech) antibody.

Immunofluorescence Double Labeling of Cells and Confocal Laser Scanning Microscopy

The cultured ice plant cells were fixed in 3.7% paraformaldehyde in 50 mM sodium phosphate buffer, pH 7.0, and 5 mM EGTA. To disperse single cells, the cells were treated with 3% cellulase for 20 min to partially digest cell walls. The plasma membrane was permeabilized with 0.5% Triton X-100 in 50 mM sodium phosphate buffer, pH 7.0, and 5 mM EGTA for 5 min. The cells were incubated in blocking buffer (phosphate-buffered saline containing 0.25% bovine serum albumin, 0.25% gelatin, 0.05% Nonidet P-40, and 0.02% sodium azide) at room temperature. The primary antibodies including affinity-purified polyclonal antibodies (mcSKD1, mEH, AtTLG2a, VSR, BP-80, and V-type ATPase B1) were used at a dilution of one-tenth in blocking buffer and incubated for 1 h. After washing with blocking buffer three times for 30 min, the cells were incubated with secondary antibodies anti-mouse IgG conjugated to rhodamine and anti-rabbit IgG conjugated to FITC (Jackson Immuno-Research) at a dilution of 1/100.

A Zeiss LSM 510 laser scanning confocal microscope equipped with a water objective was used to examine the labeled cells. The confocal scanner used excitation argon laser and the beam splitter HFT UV/488/543/633. Filters BP500-530IR and LP560 collected the emitted fluorescence. Fifteen to twenty-five cells were scanned for each treatment. The images were collected sequentially from the same optical section, analyzed by Zeiss LSM Browers, and quantified by Adobe Photoshop 7.0 software. The magenta (M) and white (W) pixel areas in single sections were measured and the percent of mcSKD1 colocalized with various membrane markers was defined as W/M.

Immunogold Labeling

Ultrathin sections (70 nm) were obtained from salt-treated ice plant leaves, roots, and callus and were collected on formvar-coated nickel grids according to Chung et al. (2002). The labeling was performed as previously described (Yen et al., 2001) with minor modifications. The sections were floated with the tissue-containing side downward on a droplet of blocking solution (100 mM Tris-HCl, pH 7.5, 15 mM NaCl, 1% bovine serum albumin, 0.3% Tween 20, and 0.3% Triton X-100) for 40 min, and then incubated with anti-mcSKD1 antiserum diluted to 1/200 in blocking solution for 1 h. After washing five times in distilled deionized water, sections were incubated with anti-Rabbit IgG conjugated 18-nm gold (Sigma) diluted 1/20 for 30 min. The sections were poststained with 2.5% uranyl acetate for 20 min and lead citrate (80.3 mM lead nitrate, 136.4 mM sodium citrate, and 0.16 N NaOH) for 10 min. Sections were examined using transmission electron microscopy (CM100, Philips Electron Optics).

Sequence data from this article can be found in the EMBL/GenBank data libraries under accession number AF165422.

LITERATURE CITED

Babst M, Katzmann DJ, Estepa EJ, Meerloo T, Emr SD (2002) ESCRT-III: an endosome-associated heterooligomeric protein complex required for MVB sorting. Dev Cell **3:** 271–282

Babst M, Wendland B, Estepa EJ, Emr SD (1998) The Vps4p AAA ATPase regulates membrane association of a Vps protein complex required for normal endosome function. EMBO J **17:** 2982–2993

Barkla BJ, Vera-Estrella V, Camacho-Emiterio J, Pantoja O (2002) Na$^+$/H$^+$ exchange in the halophyte *Mesembryanthemum crystallinum* is associated with cellular sites of Na$^+$ storage. Funct Plant Biol **29:** 1017–1024

Barkla BJ, Zingarelli L, Blumwald E, Smith JAC (1995) Tonoplast Na$^+$/H$^+$ antiport activity and its energization by the vacuolar H$^+$-ATPase in the halophytic plant *Mesembryanthemum crystallinum* L. Plant Physiol **109:** 549–556

Bassham DC, Sanderfoot AA, Kovaleva V, Zheng H, Raikhel NV (2000) AtVPS45 complex formation at the *trans*-Golgi network. Mol Biol Cell **11:** 2251–2265

Bishop N, Woodman P (2000) ATPase-defective mammalian VPS4 localizes to aberrant endosomes and impairs cholesterol trafficking. Mol Biol Cell **11:** 227–239

Bolte S, Brown S, Satiat-Jeunemaitre B (2004) The *N*-myristoylated Rab-GTPase m-Rab$_{mc}$ is involved in post-Golgi trafficking events to the lytic vacuole in plant cells. J Cell Sci **117:** 943–954

Bolte S, Schiene K, Dietz K-J (2000) Characterization of a small GTP-binding protein of the rab 5 family in *Mesembryanthemum crystallinum* with increased level of expression during early salt stress. Plant Mol Biol **42:** 923–936

Chung MC, Chou SJ, Kuang LY, Charng YY, Yang SF (2002) Subcellular localization of 1-aminocyloprrane-1-carboxylic acid oxidase in apple fruit. Plant Cell Physiol **43:** 549–554

Cushman JC (2001) Crassulacean acid metabolism: a plastic photosynthetic adaptation to arid environments. Plant Physiol **127:** 1439–1448

Epimashko S, Meckel T, Fischer-Schliebs E, Lüttge U, Thiel G (2004) Two functionally different vacuoles for static and dynamic purposes in one plant mesophyll leaf cell. Plant J **37:** 294–300

Frickey T, Lupas AN (2004) Phylogenetic analysis of AAA proteins. J Struct Biol **146:** 2–10

Galteau M-M, Antoine B, Reggio H (1985) Epoxide hydrolase is a marker for the smooth endoplasmic reticulum in rat liver. EMBO J **4:** 2793–2800

Geelen D, Leyman B, Batoko H, Di Sansabastiano G-P, Moore I, Blatt MR (2002) The abscisic acid-related SNARE homolog NtSyr1 contributes to secretion and growth: evidence from competition with its cytosolic domain. Plant Cell **14:** 387–406

Golldack D, Dietz K-J (2001) Salt-induced expression of the vacuolar H$^+$-ATPase in the common ice plant is developmentally controlled and tissue specific. Plant Physiol **125:** 1643–1654

Hafke JB, Hafke Y, Smith JAC, Lüttge U, Thiel G (2003) Vacuolar malate uptake is mediated by an anion-selective inward rectifier. Plant J **35:** 116–128

Hanson PI, Whiteheart SW (2005) AAA+ proteins: have engine, will work. Nat Rev Mol Cell Biol **6:** 519–529

Hara-Nishimura I, Shimada T, Hatano K, Takeuchi Y, Nishimura M (1998) Transport of storage vacuoles is mediated by large precursor-accumulating vesicles. Plant Cell **10:** 825–836

Herman EM, Li X, Su RT, Larsen P, Hsu H, Sze H (1994) Vacuolar-type H$^+$-ATPases are associated with the endoplasmic reticulum and provacuoles of root tip cells. Plant Physiol **106:** 1313–1324

Hislop JN, Marley A, von Zastrow M (2004) Role of mammalian vacuolar protein-sorting proteins in endocytic trafficking of a non-ubiquitinated G protein-coupled receptor to lysosomes. J Biol Chem **279:** 22522–22531

Jou Y, Chou P-H, He M, Hung Y, Yen HE (2004) Tissue-specific expression and functional complementation of a yeast potassium-uptake mutant by a salt-induced ice plant gene *mcSKD1.* Plant Mol Biol **54:** 881–893

Katzmann DJ, Odorizzi G, Emr SD (2002) Receptor downregulation and multivesicular-body sorting. Nat Rev Mol Cell Biol **3:** 893–905

Kluge C, Lamkemeyer P, Tavakoli N, Golldack D, Kandlbinder A, Dietz K-J (2003) cDNA cloning of 12 subunits of the V-type ATPase from *Mesembryanthemum crystallinum* and their expression under stress. Mol Membr Biol **20:** 171–183

Kramer D (1979) Ultrastructural observations on developing leaf bladder cells of *Mesembryanthemum crystallinum* L. Flora **168:** 193–204

Levine A (2002) Regulation of stress responses by intracellular vesicle trafficking? Plant Physiol Biochem **40:** 531–535

Leyman B, Geelen D, Blatt MR (2000) Localization and control of expression of Nt-Syr1, a tobacco snare protein. Plant J **24:** 369–381

Leyman B, Geelen D, Quintero FJ, Blatt MR (1999) A tobacco syntaxin with a role in hormonal control of guard cell ion channels. Science **283:** 537–540

Lin Y, Kimpler LA, Naismith TV, Lauer JM, Hanson PI (2005) Interaction of the mammalian endosomal sorting complex required for transport (ESCRT) III protein hSnf7-1 with itself, membrane, and the AAA+ ATPase SKD1. J Biol Chem **280:** 12799–12809

Martin A, Baker TA, Sauer RT (2005) Rebuilt AAA+ motors reveal operating principles for ATP-fuelled machines. Nature **437:** 1115–1120

Mazel A, Leshem Y, Tiwari BS, Levine A (2004) Induction of salt and osmotic stress tolerance by overexpression of an intracellular vesicle trafficking protein AtRab7 (AtRabG3e). Plant Physiol **134:** 118–128

Meyer HH (2005) Golgi reassembly after mitosis: the AAA family meets the ubiquitin family. Biochim Biophys Acta **1744:** 108–119

Périer F, Coulter KL, Liang H, Radeke CM, Garber RF, Vandenberg CA (1994) Identification of a novel mammalian member of the NSF/CDC48p/Pas1p/TBP-1 family through heterologous expression in yeast. FEBS Lett **351:** 286–290

Pratelli R, Sutter J-U, Blatt MR (2004) A new catch in the SNARE. Trends Plant Sci **9:** 187–195

Ratajczak R (2000) Structure, function and regulation of the plant vacuolar H$^+$-translocating ATPase. Biochim Biophys Acta **1465:** 17–36

Rockel B, Ratajczak R, Becker A, Lüttge U (1994) Changed densities and diameters of intra-membrane tonoplast particles of *Mesembryanthemum crystallinum* in correlation with NaCl-induced CAM. J Plant Physiol **143:** 318–324

Römisch K (2005) Endoplasmic reticulum-associated degradation. Annu Rev Cell Dev Biol **21:** 435–456

Scheuring S, Bodor O, Röhricht RA, Müller S, Beyer A, Köhrer K (1999) Cloning, characterisation, and functional expression of the *Mus musculus SKD1* gene in yeast demonstrates that the mouse *SKD1* and the yeast *VPS4* genes are orthologues and involved in intracellular protein trafficking. Gene **234:** 149–159

Scott A, Chung H-Y, Gonciarz-Swiatek M, Hill GC, Whitby FG, Gaspar J, Holton JM, Viswanathan R, Ghaffarian S, Hill CP, et al (2005) Structural and mechanistic studies of VPS4 proteins. EMBO J **24:** 3658–3669

Seidel T, Kluge C, Hanitzsch M, Roß J, Sauer M, Dietz K-J, Golldack D (2004) Colocalization and FRET-analysis of subunits c and a of the vacuolar H$^+$-ATPase in living plant cells. J Biotechnol **112:** 165–175

Sianidis G, Karamanou S, Vrontou E, Boulias K, Repanas K, Kyrpides N, Politou AS, Economou A (2001) Cross-talk between catalytic and regulatory elements in a DEAD motor domain is essential for SecA function. EMBO J **20:** 961–970

Slesak I, Miszalski Z, Karpinska B, Niewiadomska E, Ratajczak R, Karpinski S (2002) Redox control of oxidative stress responses in the C3-CAM intermediate plant *Mesembryanthemum crystallinum.* Plant Physiol Biochem **40:** 669–677

Treichel S (1986) The influence of NaCl on Δ–pyrroline-5-carboxylate reductase in proline-accumulating cell suspension cultures of *Mesembryanthemum nodiflorum* and other halophytes. Physiol Plant **67:** 173–181

Tse YC, Mo B, Hillmer S, Zhao M, Lo SW, Robinson DG, Jiang L (2004) Identification of multivesicular bodies as prevacuolar compartments in *Nicotiana tabacum* BY-2 cells. Plant Cell **16:** 672–693

Yen HE, Wu S-M, Hong Y-H, Yen S-K (2000) Isolation of 3 salt-induced low-abundance cDNAs from light-grown callus of *Mesembryanthemum crystallinum* by suppression subtractive hybridization. Physiol Plant **110:** 402–409

Yen S-K, Chung M-C, Chen P-C, Yen HE (2001) Environmental and developmental regulation of a wound-induced cell wall protein WI12 in halophyte *Mesembryanthemum crystallinum.* Plant Physiol **127:** 517–528

Yeo SCL, Xu L, Ren J, Boulton VJ, Wagle MD, Liu C, Ren G, Wong P, Zahn R, Sasajala P, et al (2003) Vps20p and Vta1p interact with Vps4p and function in multivesicular body sorting and endosomal transport in *Saccharomyces cerevisiae.* J Cell Sci **116:** 3957–3970

Zerial M, McBride H (2001) Rab proteins as membrane organizers. Nat Rev Mol Cell Biol **2:** 107–119

Zhu G, Zhai P, Liu J, Terzyan S, Li G, Zhang XC (2004) Structural basis of Rab5-Rabaptin5 interaction in endocytosis. Nat Struct Mol Biol **11:** 975–983

Zhu J, Gong Z, Zhang C, Song C-P, Damsz B, Inan G, Koiwa H, Zhu JK, Hasegawa PM, Bressan RA (2002) OSM1/SYP61: a syntaxin protein in Arabidopsis controls abscisic acid-mediated and non-abscisic acid-mediated responses to abiotic stress. Plant Cell **14:** 3009–3028

Zhu JK (2001) Plant salt tolerance. Trends Plant Sci **6:** 66–71